Peter, L.M. (2013) Energetics and kinetics of light-driven oxygen evolution at semiconductor electrodes:the example of hematite. Journal of Solid State Electrochemistry, 17 (2). pp. 315-326. ISSN 1432-8488

Link to official URL (if available): http://dx.doi.org/10.1007/s10008-012-1957-3

The original publication is available at www.springerlink.com

Opus: University of Bath Online Publication Store

http://opus.bath.ac.uk/

This version is made available in accordance with publisher policies. Please cite only the published version using the reference above.

See http://opus.bath.ac.uk/ for usage policies.

Please scroll down to view the document.

Energetics and kinetics of light-driven oxygen evolution at semiconductor electrodes: the example of hematite

Laurence M Peter

Department of Chemistry, University of Bath, Bath BA2 7AY, United Kingdom

Phone +44(0)1225 386502
e-mail: l.m.peter@bath.ac.uk

Dedicated to Professor Alexander Milchev on the occasion of his 70th birthday

Abstract

Light-driven water splitting (photoelectrolysis) at semiconductor electrodes continues to excite interest as a potential route to produce hydrogen as a sustainable fuel, but surprisingly little is known about the kinetics and mechanisms of the reactions involved. Here some basic principles of semiconductor photoelectrochemistry are reviewed with particular emphasis on the effects of slow interfacial electron transfer at n-type semiconductors in the case of light-driven oxygen evolution. A simple kinetic model is outlined that considers the competition between interfacial transfer of photogenerated holes and surface recombination. The model shows that if interfacial charge transfer is very slow, the build-up of holes at the surface will lead to substantial changes in the potential drop across the Helmholtz layer, leading to non-ideal behaviour (Fermi level pinning). The kinetic model is also used to predict the response of photoanodes to chopped illumination and to periodic perturbations of illumination and potential. Recent experimental results obtained for α-Fe_2O_3 (hematite) photoanodes are reviewed and interpreted within the framework of the model.

Keywords

hematite, impedance, IMPS, oxygen evolution, photoelectrolysis, tandem cell, water splitting

Introduction

Light-driven water splitting or photoelectrolysis remains the holy grail of photo-electrochemistry. Forty years after Fujishima and Honda published their seminal Nature paper on photoelectrolysis of water at single crystal rutile (TiO_2) electrodes [1], the quest for efficient stable low-cost systems for light-driven water splitting continues. The energetic criteria for efficient photoelectrolysis are well understood [2], but suitable stable semiconductor materials that fulfil these criteria have proved elusive. The main problem is that semiconductors with electron affinities that are small enough to allow transfer of electrons from the conduction band to protons in solution are either unstable under illumination (e.g. II-VI and III-V semiconductors) or have such high band gaps (E_g) that light absorption only occurs in the UV (e.g. TiO_2, $SrTiO_3$). Stable n-type transition metal oxides such as WO_3 and Fe_2O_3 that absorb visible light have conduction band energy levels that lie below the H^+/H_2 redox Fermi energy, so that an additional bias voltage is needed to enable photoelectrolysis. This bias voltage can be provided by a solar cell placed behind the photoanode, where it absorbs long wavelength light transmitted through the photoanode. This arrangement, which is shown in Fig. 1a, is referred to as a tandem photoelectrolysis cell [3].

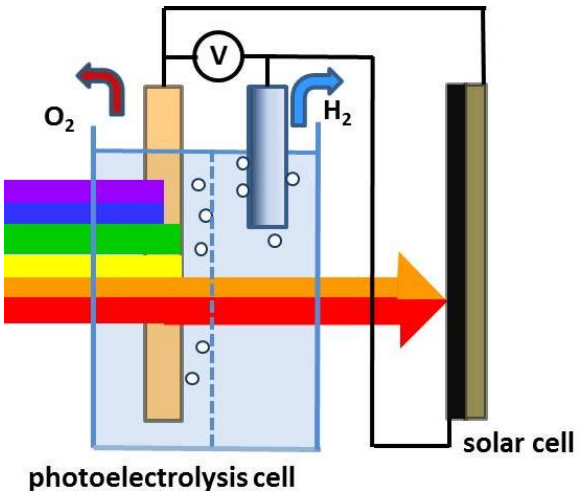

(a)

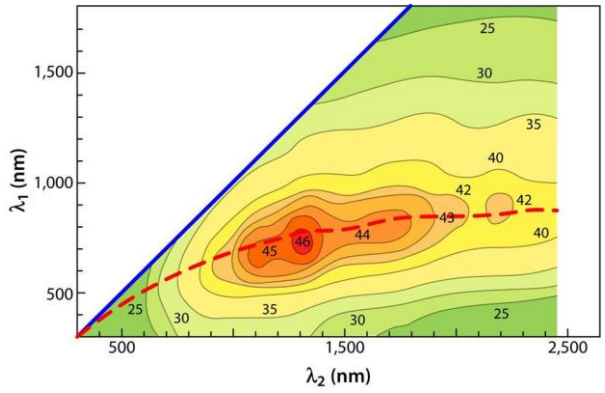

(b)

Figure 1. (a) Tandem photoelectrolysis cell for light-driven water splitting. The solar cell absorbs long wavelength light transmitted through the photoanode, generating a bias voltage (V) that is applied to the photoelectrolysis cell in order to raise the Fermi level of the cathode above the H^+/H_2 redox potential. (b) Contour plot showing the maximum theoretical efficiency as a function of the absorption onset of the photoanode (*y*-axis) and of the solar cell (*x*-axis). The dashed line indicates the ideal situation where the currents of the two absorbers are equal (figure courtesy A.J. Nozik).

The theoretical efficiency of this type of tandem arrangement has been discussed by Bolton et al. [4]. Fig. 1b is a contour plot that shows the theoretical efficiency of a tandem cell photoelectrolysis cell configuration for the case where there are no energy losses (the interested reader is referred to the ref [4] for details of other calculations that involve assumptions about the magnitude of energy losses in the system). The dotted line corresponds to the ideal situation in which the currents of the photoelectrolysis cell and the solar cell are matched. The figure shows that optimum performance should be obtained using a photoanode with an absorption edge between 550 nm (2.25 eV) and 700 nm (1.77 eV) in tandem with a solar cell with a corresponding absorption edge range between 850 nm (1.46 eV) and 1100 nm (1.13 eV). α-Fe_2O_3 (hematite), which has a band gap of around 2.0 eV, is therefore a suitable material that could be combined with a low cost solar cell based on a semiconductor with E_g in the range 1.2 - 1.4 eV.

Hematite has been studied extensively as a potential photoanode for a tandem photoelectrolysis cell, but although considerable progress has been made in optimizing electrode morphology and surface properties, remarkably little quantitative information is available about the factors that control the performance of hematite electrodes. In particular, it is only recently that the implications of the extremely slow kinetics of the light-driven oxygen evolution reaction (LOER) are becoming clearly understood. The oxidation of water

is a 4 electron process, and the energetically favoured pathway will depend on the surface chemistry of the photoanode material. In the case of TiO_2 or WO_3 photoanodes, the metal is already in its highest oxidation state, so that the pathway cannot involve oxidation of metal atoms in the surface. Instead it is likely to involve surface peroxo and superoxo species.[5,6]. By contrast, the Fe(III) state in Fe_2O_3 can in principle be oxidized to any of the known higher oxidation states: Fe(IV), Fe(V) and Fe(VI), and oxygen evolution could involve cycling of the oxidation state of Fe surface atoms as well as formation of peroxo and superoxo species. It has become clear from recent studies [7,8,9,10,11,12,13,14] that there must be a kinetic bottleneck in the LOER mechanism in the case of hematite, indicating a high activation energy for at least one of the elementary steps.

The purpose of the present paper is to review briefly some fundamental concepts of photoelectrochemistry before outlining a simple model to describe the kinetics of the LOER, which can be thought of as the interfacial electron transfer of photogenerated holes. This model is then used as the basis for a phenomenological description of the response of the photoelectrode to steady state, transient and periodic illumination as well as to periodic potential perturbation under steady state illumination. Recent kinetic results obtained for hematite electrodes are reviewed, and the data are used to draw conclusions about some of the problems that currently limit the performance of the material.

Energetics of Light-Driven Water Splitting

The energetics of light-driven water splitting is best understood in terms of free energy. The free energies of electrons and holes in an illuminated semiconductor are equivalent to the respective quasi Fermi levels. Under illumination with light with energy $h\upsilon > E_g$, excitation of electrons from the valence band to the conduction band establishes a non-equilibrium steady state population of electrons (n) and holes (p). The electrons and holes are assumed to be in thermal equilibrium with the lattice, so that the Fermi Dirac statistics apply. The electron and hole concentrations are given by

$$n = N_c \left(\frac{1}{1+\exp\left(\frac{E_c - {}_n E_F}{k_B T} \right)} \right) \qquad p = N_v \left(\frac{1}{1+\left(\frac{{}_p E_F - E_v}{k_B T} \right)} \right) \tag{1}$$

where E_c, E_v are the conduction and valence band energies, ${}_nE_F$, ${}_pE_F$ are the quasi Fermi levels for electrons and holes and N_c, N_v are the conduction and valence band densities of states. If we consider an n-type semiconductor like hematite, the equilibrium hole density in the dark is very low since $n_{eq} >> p_{eq}$. Illumination creates equal excess concentrations (Δn and Δp) of electrons in the conduction band and holes in the valence band. For an n-type semiconductor, $n_{eq} + \Delta n \approx n_{eq}$, so that ${}_nE_F$ is almost the same as in the equilibrium Fermi level E_F in the dark. However, since $p_{eq} + \Delta p >> p_{eq}$, the quasi Fermi level for holes is displaced downwards towards the valence band, increasing the driving force for oxidation reactions. In the case of water oxidation in the LOER, the driving force for the reaction is determined by the free energy difference between ${}_pE_F$ at the surface and the equilibrium redox Fermi level for the O_2/H_2O couple, which corresponds to the equilibrium (Nernstian) electrode potential. This situation is illustrated in Fig. 2 for the case of an n-type electrode that has been biased into depletion and where slow electron transfer kinetics leads to a build-up of holes at the interface, driving ${}_pE_F$ below $E_F(O_2/H_2O)$. The difference in free energies ΔE_F, which is a measure of the driving force, can be used to define the overpotential for the oxidation of water: $\eta_a = \Delta E_F/q$. Fig. 2 also illustrates the energetics of the cathode. Application of a bias voltage raises the Fermi level of the metal cathode sufficiently far above the equilibrium Fermi level for the H^+/H_2 couple to produce the required current.

It should be noted at this point that the concept of 'overpotential' is different at the two electrodes in the photoelectrolysis cell. Provided that the photoanode is not too highly doped and behaves ideally, the change in free energy of holes (${}_pE_F$) in the is associated with the entropic (i.e. concentration) part of the Gibbs energy: the internal energy contribution remains constant, provided that the potential drop across the Helmholtz layer does not change. By contrast, the change in free energy of electrons (Fermi level shift) in the metal cathode is associated with the change in potential drop across the Helmholtz layer. This difference is not always understood in the literature, where it is not uncommon to see the Butler Volmer equation used to describe the kinetics of minority carrier transfer at semiconductor electrodes. This is incorrect, since the activation energy for interfacial minority carrier transfer is not affected by changes in the quasi Fermi level unless the potential drop across the Helmholtz layer also changes, as is the case for highly doped semiconductors. When the quasi Fermi level (and hence the overpotential) changes, the rate constant remains the same and only the concentration of reacting minority carriers changes. The situation is different at the metal cathode. Changes in overpotential alter the potential

drop across the Helmholtz layer, changing the activation energy and hence the rate constant for electron transfer: the concentration of reacting electrons in the metal is effectively constant.

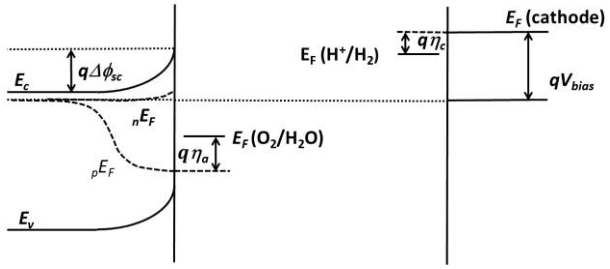

Figure 2. Splitting of the quasi Fermi levels for an illuminated n-type semiconductor such as hematite biased into depletion (band bending = $q\Delta\phi_{sc}$). The difference between $_pE_F$ and E_F (O_2/H_2O) defines the overpotential η_a for the oxygen evolution reaction. In the case shown here, η_a is large due the accumulation of holes at the interface as a consequence of sluggish electron transfer kinetics. As shown below, $_pE_F$ may be displaced into the valence band if the rate constant for charge transfer is sufficiently slow. In order to achieve water splitting, an additional bias voltage is required to raise the Fermi level of the metal cathode above $E_F(H^+/H_2)$. In the figure, the overpotential for the cathodic reaction, η_c is exaggerated for clarity. If catalytic electrodes like platinum are used, the cathodic overpotential will be much smaller.

Kinetics: the steady state

Electron-hole pairs generated by light absorption can either recombine or they can be separated, giving rise to a steady state photocurrent. In the case of the n-type semiconductor shown in Fig. 2, holes reaching the surface can drive the 4-electron oxidation of water. In alkaline solution, this process is described by equation 2.

$$4\ OH^- + 4\ h^+ \rightarrow 2H_2O + O_2 \qquad (2)$$

Although the elementary steps involved in this process are still the subject of speculation, a phenomenological approach based on overall rates can be used to express the competition between interfacial charge transfer and recombination [15].

Light-driven electrode reactions at semiconductor electrodes always have to compete with electron-hole recombination. Recombination may take place either in the bulk of the semiconductor or at the surface. In the bulk, where majority carriers (electrons for an n-type semiconductor) are in large excess, recombination determines the minority carrier (hole) lifetime. The hole lifetime, τ_p, and the hole diffusion coefficient define the hole diffusion length, L_p:

$$L_p = \sqrt{D_p \tau_p} \tag{3}$$

L_p is very small (nm) for highly doped and defective semiconductors like hematite.

Near the surface of the semiconductor, where the quasi Fermi levels are separated by illumination as shown in Fig. 2, the gradients of ${}_nE_F$ and ${}_pE_F$ determine the fluxes of electrons towards the bulk and of holes towards the surface respectively. In the model of depletion layer photocurrents developed originally by Gärtner [16] for solid state junctions and extended to semiconductor/electrolyte junctions by Wilson [17] and by Butler [18], it is assumed that all holes that reach the edge of the space charge region at $x = W$ (where W is width of the space charge region) are transferred to the contacting phase (i.e. no recombination occurs in the space charge region or at the surface). This assumption gives rise to the boundary condition that the excess hole concentration Δp at $x = W$ is zero. However, this approximation will no longer be valid if electron transfer at the interface is slow, leading to a build-up of holes. A more realistic approach that includes the effects of recombination of electrons and holes in the space charge region as well as the influence of the rate of interfacial charge transfer has been given by Reichmann [19], and El Guibaly and Colbow have extended this treatment to include surface recombination [20]. The increasing complexity of these models and the absence of reliable values for the variables probably explain why these extensions of the basic Gärtner model have not been followed up extensively in the literature. In the present paper, a much simpler phenomenological approach is taken that leads to a semi-quantitative understanding of the behaviour of holes at photoanode like hematite.

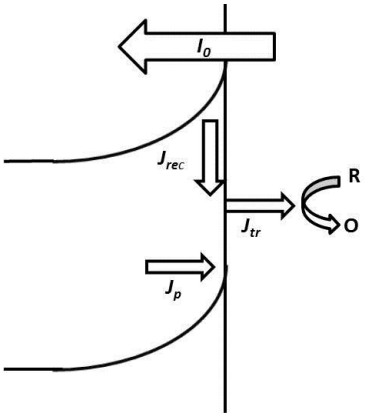

Figure 3. Balance of steady state photon (I_0), hole (J_p) and electron (J_{rec}) fluxes into the semiconductor/ electrolyte interface. J_{tr} is the flux of holes taking part in interfacial electron transfer to oxidize solution species.

The starting point for the model is Fig. 3, which shows the situation for an n-type semiconductor with a defined space charge region (it should be noted this model will not apply to mesoporous films). Steady state illumination produces a flux J_p of holes into the surface that corresponds to a fraction $f_p\ I_0$ of the absorbed photon flux I_0 that is determined by the penetration depth of the light, the width of the space charge region and losses due to recombination in the bulk and space charge regions. In the steady state, J_p is balanced by the sum of two fluxes of holes out of the surface. The first, J_{tr}, is the flux of holes across the interface (equal in magnitude to the flux of electrons transferred from solution redox species to the valence band). The second, J_{rec}, is the flux of holes due to surface (or near surface [21]) recombination. The flux of holes taking part in surface recombination, J_{rec}, must equal to the flux of electrons into the surface J_n. This simple model gives the external quantum efficiency, *EQE*, as

$$EQE = f_p \frac{J_{tr}}{J_{tr} + J_{rec}} = f_p \frac{k_{tr}}{k_{tr} + k_{rec}} \tag{4}$$

The concentration of holes per unit area, p_{surf}, is determined by the ratio

$$p_{surf} = \frac{f_p I_0}{\left(k_{tr} + k_{rec}\right)} \tag{5}$$

Here the pseudo first order rate constant k_{rec} depends on the volume concentration of electrons, $n_{x=0}$, at the surface, the electron capture cross section of holes, σ_p and the thermal velocity of electrons, υ_{th} :

$$k_{rec} = \sigma_p \upsilon_{th} n_{x=0} \tag{6}$$

In the non-degenerate limit where Boltzmann statistics apply, the concentration of electrons at the surface depends on the doping density, N_d, and the band bending $q\Delta\phi_{sc}$ shown in Fig. 2.

$$n_{x=0} = N_d e^{-\frac{q\Delta\phi_{sc}}{k_B T}} \tag{7}$$

so that the recombination rate decreases as the band bending increases. The recombination rate constant rate constant can therefore be expressed in the form

$$k_{rec} = \sigma_p \upsilon_{th} N_d e^{-\frac{q\Delta\phi_{sc}}{k_B T}} = k_{rec}^0 e^{-\frac{q\Delta\phi_{sc}}{k_B T}} \tag{8}$$

In order to obtain an order of magnitude estimate of $k_{\mathrm{rec}}{}^0$ for hematite, let us take $N_d = 10^{19}$ cm^{-3}, $\upsilon_{th} = 10^5$ cm s^{-1} and $\sigma_p = 10^{-16}$ cm^2. This gives $k_{rec}{}^0 = 10^8$ s^{-1}.

For the purposes of obtaining current voltage plots for qualitative illustration, it will be assumed that recombination in the space charge region can be neglected. In this case, the fraction of photogenerated holes that is collected can be approximated by the Gärtner expression

$$f_p = 1 - \frac{e^{-\alpha W}}{1 + \alpha L_p} \tag{9}$$

Here W is the width of the space charge region, α is the optical absorption coefficient of the semiconductor and L_p is the hole diffusion length defined by equation 3. In the limit where no surface recombination takes place, the *EQE* becomes identical with f_p.

This simple model suffices to show that sluggish electron transfer and recombination (low values of k_{tr} and k_{rec}) will result in the build-up of a substantial concentration of holes at the surface. This will alter the potential distribution across the interface, which can be divided into the potential drop across the space charge region, $\Delta\phi_{sc}$, and the potential drop across the Helmholtz layer, $\Delta\phi_H$. If we treat the accumulated holes as a surface charge, the decrease in potential drop across the space charge layer is given by

$$\delta\Delta\phi_{sc} = -\delta\Delta\phi_H = -\frac{qp_{surf}}{C_H + C_{sc}} \tag{10}$$

Some general features of photoanode behaviour can be predicted from this model. If k_{tr} is small, hole accumulation will lead to the electrode behaving more like a metal in the photocurrent onset region, where the rate of hole accumulation is highest. This effect, which is known as Fermi level pinning, means that most of any change in applied potential appears across the Helmholtz layer and not across the space charge region. This will change the activation energy for interfacial electron transfer, and hence k_{tr}.

Fig. 4 illustrates the large displacement of the photocurrent onset that is expected if charge transfer during light-driven oxygen evolution is sluggish. As discussed in more detail below, this is the case for α-Fe_2O_3 electrodes, where k_{tr} has been measured to be less than 10^2 s^{-1} [12,22]. The reason for the displacement is that in order to transfer holes efficiently across the surface, the band bending needs to be sufficiently large to ensure that k_{rec} becomes smaller than k_{tr}. The partial Fermi level pinning effect can be seen in the calculated plot of $\Delta\phi_{sc}$ vs. applied potential, which exhibits an inflection in the photocurrent onset region.

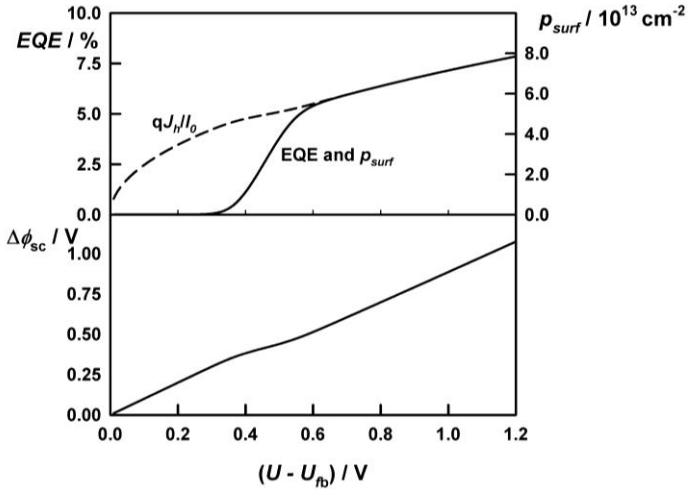

Figure 4. The upper plot shows the normalized hole flux predicted by the Gärtner equation (broken line) and the large displacement of the EQE plot (continuous line) in the presence of surface recombination. The right hand y-axis indicates the surface hole concentration. The lower plot shows the change in the applied potential across the space charge layer. Partial Fermi level pinning due to the build-up of holes at the surface is evident from the inflection in the $\Delta\phi_{sc}$ plot in the photocurrent onset region. Values used in the calculation: $k_t = 10$ s^{-1}, $\alpha = 1.5 \times 10^5$ cm^{-1}, $N_d = 10^{19}$ cm^{-3}, $\varepsilon = 15$, $C_H = 100$ μF cm^{-2}, $\sigma_p = 10^{-16}$ cm^2, $\upsilon_{th} = 10^5$ cm s^{-1}, $I_0 = 10^{16}$ cm^{-2} s^{-1}.

Under illumination of the photoanode, the build-up of holes at the surface pushes ${}_pE_F$ down towards the valence band. In order to illustrate this effect, it is necessary to convert the surface concentration of holes (cm^{-2}) into an order of magnitude volume concentration. Numerical calculations [23] suggest that the effective thickness, δ, of the region where minority carriers build up is of the order of a few nm, so that to a first approximation we can divide p_{surf} (cf. eqn. 5) by δ = 1nm . If charge transfer is slow enough, the Fermi level will be pushed into the valence band, and the electrode will behave more like a metal, with most of the change in applied potential appearing across the Helmholtz layer. In this extreme case η_a will no longer be dominated by the concentration term but instead by the change in activation energy for electron transfer. Fig. 5 shows that this situation for hematite, where the rate constant for charge transfer is typically less than 100 s^{-1}[12,22,24,25]. The hole quasi Fermi level moves towards the valence band as holes accumulate, and the overpotential starts to saturate at a value corresponding the energy difference between the O_2/H_2O redox Fermi level and the valence band energy. Although this calculation involves an order of magnitude approximation, it suffices to show that the large displacement of ${}_pE_F$ due to accumulation of holes is likely to lead to quasi-metallic behaviour.

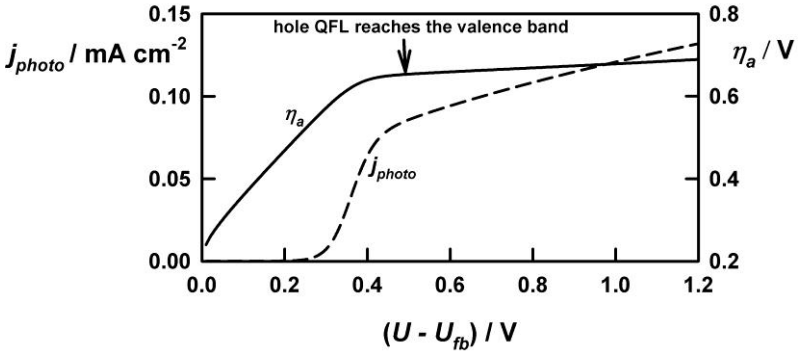

Figure 5. Overpotential as a function of electrode potential for light-driven oxygen evolution calculated for a hematite electrode for the case of slow hole transfer. The plot shows that the overpotential increases as holes build up at the interface and the quasi Fermi level (QFL) moves downwards until it enters the valence band (degenerate condition). An order of magnitude value for the volume concentration of holes has been estimated from the surface concentration p_{ss} in Fig. 4 by assuming that they are located in a 1 nm thick surface layer. Values used in the calculation. $E_F(O_2/H_2O - E_v) = 0.65$ eV, $N_V = 10^{20}$ cm^{-3}, $k_{tr} = 10^2$ s^{-1}. The other values used in the calculation are the same as those used for Fig. 4. Note that it is assumed that all holes are located in the valence band.

This discussion raises an interesting question about the description of holes at the surface. In the simple model outlined above, the surface concentration of holes is derived using a purely kinetic argument, and the assumption that these holes are located in the valence band was used to derive the position of the hole QFL. However, semiconductor/ electrolyte interfaces are rarely ideal, and there are generally electronic states at the surface that have energies in the band gap. These surface states can capture electrons and holes, giving rise to surface recombination. The problem with the surface state concept is that is generally assumed that the energy level is the same regardless of whether it is empty or filled with electrons. This assumption is unlikely to be valid since the coordination of surface atoms depends on their oxidation state. For example, in the case of α-Fe_2O_3 it is possible that holes could be localized on surface iron atoms leading to a change of oxidation state from Fe(III) to Fe(IV). In principle, multiple hole trapping could even lead to the formation of surface Fe (V) and Fe(VI) species. In this case, the concentration of free holes in the valence band could be much lower. Recent evidence for the formation of surface bound Fe(X) species ($3 < X \leq 6$) from cyclic voltammetry and potential modulated absorption spectroscopy [25] suggests that the redox potential of the Fe(X)/Fe(III) couple is ca. 0.4 V more positive than the O_2/H_2O redox potential and ca. 0.25 eV below the valence band edge of α-Fe_2O_3. If this is the case, then ${}_pE_F$ would be pinned at the surface as shown in Fig. 6, and the concentration of free

holes would be much lower than in the case where ${}_pE_F$ can be displaced into the valence band. More importantly, the energetics of the water oxidation process change because the reactant is no longer a hole in the valence band but a surface-bound redox species. This illustrates the dangers of using concepts from solid state physics to describe the energetics of reactions involving electron transfer at the semiconductor/electrolyte interface.

An example of several possible reaction schemes involving higher valent surface Fe species is shown below. In this case the higher valent Fe intermediate is Fe(IV)=O^-, and oxygen evolution involves a second order surface reaction. Spectroscopic evidence for higher valent intermediates has been obtained [25], but the chemical identity of the species as well as details of the elementary and rate determining steps involved in the LOER remain to be established.

$$>Fe^{III}\text{-}O^- + h^+ \rightarrow >Fe^{IV}=O$$
$$>Fe^{IV}=O + 2\,OH^- + h^+ \rightarrow >Fe^{III}\text{-}O\text{-}O^- + H_2O \qquad \textbf{Scheme 1}$$
$$2\,>Fe^{III}\text{-}O\text{-}O^- \rightarrow 2\,>Fe^{III}\text{-}O\text{-} + O_2$$

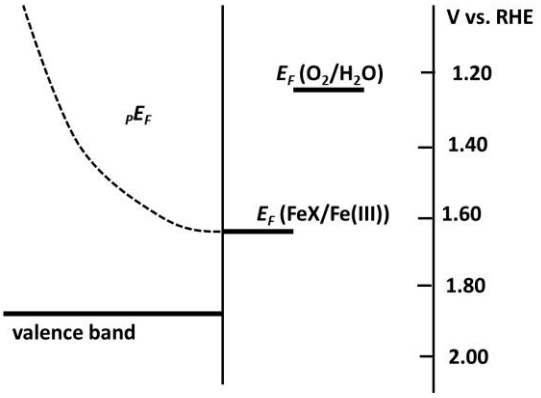

Figure 6. α-Fe_2O_3/electrolyte interface energetics showing possible pinning of hole QFL by a surface iron redox couple. The Fe(X) species here is formed by capture of holes at surface sites. The valence band position is obtained from the flat band potential of hematite and the Fe(X)/Fe(II) redox potential is obtained from the quasi-reversible couple seen in dark cyclic voltammetry of hematite electrodes [25].

Kinetics: time and frequency dependent perturbations

Transient Photocurrents

The existence of surface (and possibly also space charge) recombination processes can be deduced indirectly from the delayed onset of the photocurrent relative to the flatband

potential of photoanodes like hematite. More direct evidence for surface recombination is obtained by recording photocurrent-voltage plots under chopped illumination. In the photocurrent onset region, the photocurrent response shows a characteristic decay from a 'spike' to a steady state during the illumination period, followed by an overshoot and decay back to zero during the dark period. An example of this kind of response in the case of a hematite photoanode is shown in Fig. 7. Qualitatively, this phenomenon can be understood as follows. When the light is switched on, photogenerated electrons and holes are separated, with electrons moving towards the bulk of the semiconductor and holes towards the surface. The separation of electrons and holes charges the space charge capacitance. The corresponding 'instantaneous' displacement or charging current is not associated with charge transfer across the interface. Under continued illumination during the 'on' period, the concentration of free (or surface-trapped) holes builds up until a steady state concentration is reached at which the rate of arrival of holes is exactly balanced by interfacial transfer and recombination (cf. Fig. 3). This build-up of holes induces a recombination flux of electrons into the surface corresponding to a current of opposite sign to the hole current. In the steady state, the measured photocurrent is the sum of the hole and electron currents. When the light is switched off, the hole current falls abruptly to zero, and the current in the external circuit changes sign as electrons continue to move towards the surface to recombine with the remaining holes. Since the recombination current is linearly proportional to the surface hole concentration, the cathodic current overshoot reflects the decay of the surface hole concentration by recombination and interfacial transfer.

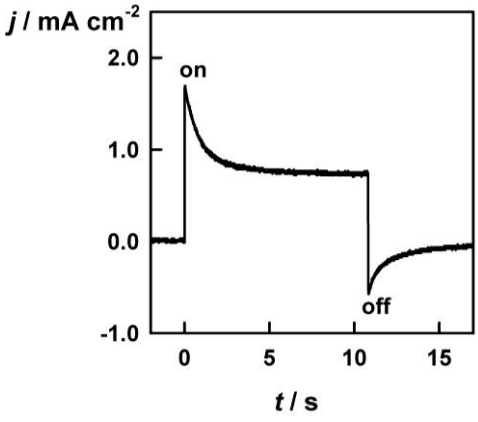

Figure 7. Transient photocurrent response of thin film α-Fe_2O_3 electrode at 0 V vs. Ag|AgCl showing the decay and overshoot characteristic of surface electron-hole recombination. Electrolyte 1.0 M NaOH.

The time-dependent solution of the problem is easily obtained.[26,27] For the 'on' transient, it takes the normalized from form

$$\frac{j(t)-j(\infty)}{j(0)-j(\infty)}=e^{-t/\tau} \tag{11a}$$

where the time constant $\tau = (k_{tr} + k_{rec})^{-1}$ and the steady state photocurrent is given by.

$$j(\infty)=\frac{k_{tr}}{(k_{tr}+k_{rec})} \tag{11b}$$

The off transient has the form

$$\frac{j(t>t_0)}{j(0)-j(t_0)}=e^{-t(k_{tr}+k_{rec})} \tag{11c}$$

The transient in Fig. 8 has been calculated for equal values of k_{tr} and k_{rec} (both 1 s^{-1}). It illustrates the main features of the transient response to chopped illumination that is commonly seen in the photocurrent onset region of electrodes such as α-Fe_2O_3 when surface recombination plays a role. It can be seen that the steady state current should increase as the potential is made more positive since the surface concentration of electrons - and hence k_{rec} – decrease as the band bending increases (cf. equation 8). Since the ratio $k_{tr}/(k_{tr} + k_{rec})$ and the sum $(k_{tr} + k_{rec})$ can be derived from experimental transients, the rate constants for charge transfer and recombination can be obtained. In practice, it is often better to use small amplitude perturbations of the illumination of the kind used in intensity-modulated photocurrent spectroscopy (IMPS) because large amplitude changes in light intensity can lead to other effects such as changes in band bending. Alternatively, small amplitude square wave modulation can be superimposed on a large background illumination level.

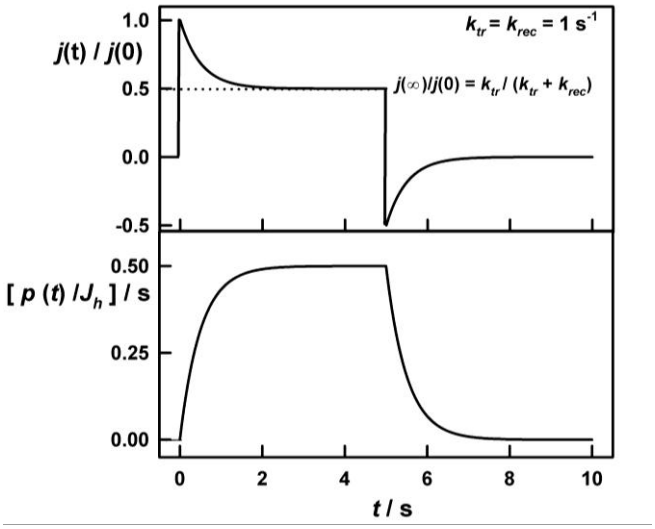

Figure 8. The upper plot shows a normalized photocurrent transient calculated for $k_{tr} = k_{rec} = 1\ s^{-1}$. Note that the steady state photocurrent $j(\infty)$ is determined by the competition between charge transfer and recombination, and the decay time constant is determined by $(k_{tr} + k_{rec})^{-1}$. Analysis of experimental transients allows the values of k_{tr} and k_{rec} to be determined. The lower plot shows the corresponding build up and decay of the surface hole concentration $p(t)$ normalized by dividing by the hole flux J_h into the surface.

Intensity Modulated Photocurrent

Intensity-modulated photocurrent spectroscopy (IMPS) [28,29,30] is a convenient way of measuring the rate constants for charge transfer and recombination. The method involves using a small sinusoidal modulation of light intensity (typically less than 10% of the dc illumination level) and measuring the phase and magnitude of the photocurrent response as a function of frequency. The result, which is usually plotted in the complex plane, can be analyzed using the simple phenomenological theory outlined above to find obtain k_{tr} and k_{rec}. These rate constants can be related to different kinetic schemes in the case of multiple electron transfer reactions ($n > 1$) [15], but the process becomes difficult for $n > 2$. The relaxation time constant $(k_{tr} + k_{rec})^{-1}$ seen in the exponential decay and overshoot of photocurrent transients gives rise to the semi-circular response shown in Fig. 9, which is described by the normalized transfer function [26]

$$\frac{j_{photo}(\omega)}{q\,J_h} = \frac{k_{tr} + i\omega}{k_{tr} + k_{rec} + i\omega} \qquad (12a)$$

The real and imaginary parts of the IMPS response are given by

$$\mathrm{Re}\left[\frac{j_{photo}(\omega)}{q\,J_h}\right] = \frac{k_{tr}\left(k_{tr}+k_{rec}\right)+\omega^2}{\left(k_{tr}+k_{rec}\right)+\omega^2} \tag{12b}$$

$$\mathrm{Im}\left[\frac{j_{photo}(\omega)}{q\,J_h}\right] = \frac{k_{rec}\omega}{\left(k_{tr}+k_{rec}\right)+\omega^2} \tag{12c}$$

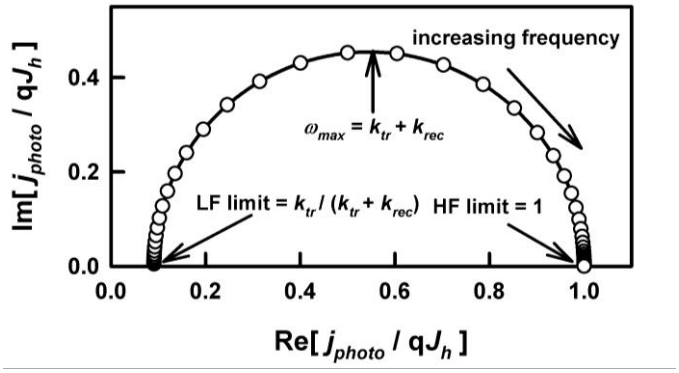

Figure 9. Normalized IMPS response showing high frequency (HF) and low frequency (LF) intercepts and maximum of the semicircle. Calculated for $k_{rec} = 10k_{tr}$.

In the high frequency (HF) limit, the real part tends towards 1 and the imaginary part towards zero. In the low frequency (LF) limit, the real part tends towards $k_{tr}/(k_{tr} + k_{rec})$. The maximum of the semicircle occurs at a radial frequency $\omega_{max} = k_{tr} + k_{rec}$. Comparison with the transient response shows the correspondence between the HF limit and the instantaneous photocurrent and the LF limit and the steady state photocurrent. The time constant of the transient response is $1/\omega_{max}$.

Both the transient and IMPS responses are affected by the *RC* time constant of the electrochemical system[26], which is determined by the series resistance, *R*, and the combination of C_{sc} and C_H. In the case of transient photocurrents, the effect of the *RC* time constant is to determine the rise time of the photocurrent. In the case of the IMPS response, the *RC* time constant gives rise to a semicircle in the lower quadrant of the complex plane as illustrated in Fig. 10. The radial frequency at the minimum of this semicircle is given by

$$\omega_{\min} = \frac{C_{sc}+C_H}{RC_{sc}C_H} \tag{13}$$

Provided that the two time constants are separated by at least an order of magnitude, then the upper semicircle can still be used to determine values of k_{tr} and k_{rec}. However, if the time

constants are closer, deconvolution becomes necessary using a value for the *RC* time constant determined, for example, by impedance.

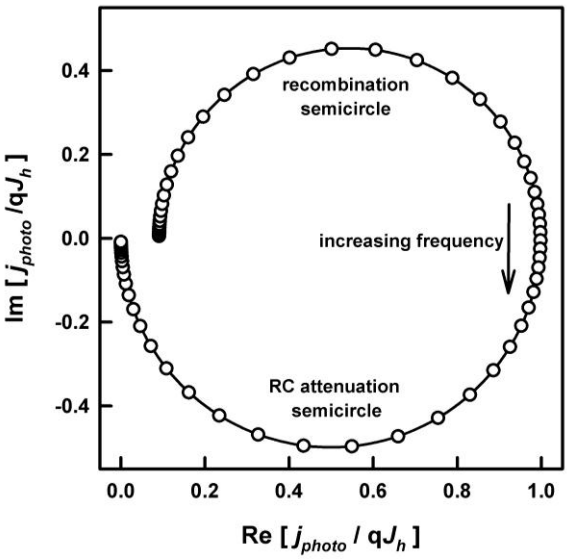

Figure 10. Complete IMPS response including the effects of RC attenuation at high frequencies. Provided that the RC time constant is much shorter than $(k_{tr} + k_{rec})^{-1}$, the upper semicircle can be used to derived the two rate constants.

Fig. 11 illustrates the kind of IMPS response that is seen for hematite film photoanodes in the photocurrent onset region where spikes appear in the chopped photocurrent. In this example, the normalized low frequency intercept is ca. 0.6 and ω_{max} is ca. 4 s^{-1}. It follows that $k_{tr} \approx 2.4\ s^{-1}$ and $k_{rec} \approx 1.6\ s^{-1}$. The values give a clear indication of how sluggish electron transfer is at hematite electrodes, even when the surface has been treated with a dilute Co(II) solution which substantially improves the current-voltage characteristics[7] (the effect of this cobalt treatment are discussed below).

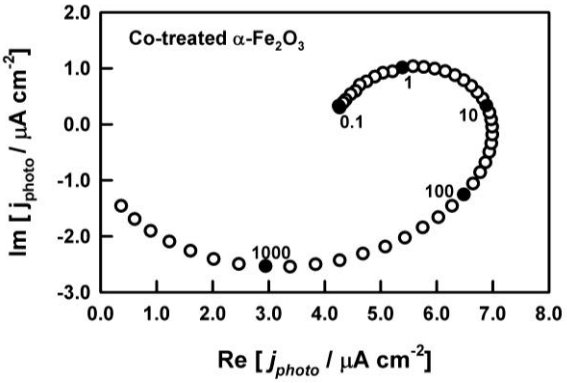

Figure 11. Experimental IMPS response measured for a thin film α-Fe_2O_3 electrode in the photocurrent onset region. The electrode was treated with a drop of 10mmM cobalt nitrate solution. Electrolyte 1.0 M NaOH. Electrode potential -0.3 V vs. Ag|AgCl. Illumination 455 nm, dc photon flux 1.1×10^{17} cm^{-2} s^{-1}.

IMPS has been used to study the potential dependence of k_{tr} and k_{rec} in the case of thin film hematite electrodes [22,24]. The results show that the semiconductor/electrode interface is very non-ideal in the case of untreated electrodes, with a substantial fraction of the applied potential change appearing across the Helmholtz layer. Treatment of the electrode with a drop of dilute Co(II) solution evidently supresses surface recombination substantially, but the electrode behaviour is still far from ideal [22,24,25].

The flattening of both semicircles that is evident in the recombination semicircle in Fig. 11 can be interpreted as evidence for a distribution of the rate constants k_{tr} and k_{rec} as a consequence of surface heterogeneity [31]. The flattening of the *RC* semicircle is attributed to the frequency-dependent permittivity of hematite [12].

Figure 12 contrasts the potential dependence of k_{tr} and k_{rec} for untreated hematite electrodes and hematite electrodes that have been treated with Co(II). The remarkable sigmoidal dependence of the two rate constants for the untreated electrode is similar to the behaviour seen for n-GaAs electrodes[31]. Since k_{tr} depends on the surface concentration of electrons, the shape of the plot reflects changes in band bending. The increase in k_{tr} above 0 V vs. Ag|AgCl corresponds to a decrease in band bending. Fermi level pinning due to the build-up of holes at the surface (or in surface states) cannot explain this effect. It seems likely that changes in the chemical composition of the surface are responsible, since they can alter the surface dipole potential, effectively changing the flat band potential. The sinusoidal change in k_{tr} tracks the k_{rec} plot and therefore probably has the same explanation: the decrease in band bending corresponds to an increase in $\Delta\phi_H$, which increases the rate constant for hole transfer by changing the activation energy. In the case of the treated electrode, the sinusoidal response is absent, and k_{tr} decreases monotonically over the entire potential range. This shows that the band bending increases monotonically with applied potential as expected. However the change in $\Delta\phi_{sc}$ estimated using eqn.8 is only 200 mV for a change in applied potential of 1 volt. This highly non-ideal behaviour suggests that most of the change in applied potential must appear across the Helmholtz layer. However, this conclusion is not supported by the fact that k_{tr} appears to fall slightly over the same potential range rather than increasing as would be expected if the increase in $\Delta\phi_H$ increases k_{tr}. Clearly the kinetics of recombination and charge transfer are more complicated than the simple treatment given here. This is not surprising, since oxygen evolution is a four electron process that involves intermediate species and a series of elementary steps. Further indications of this complexity

are provided by the observation that both k_{tr} increases linearly with light intensity, whereas k_{rec} exhibits a square root dependency [12].

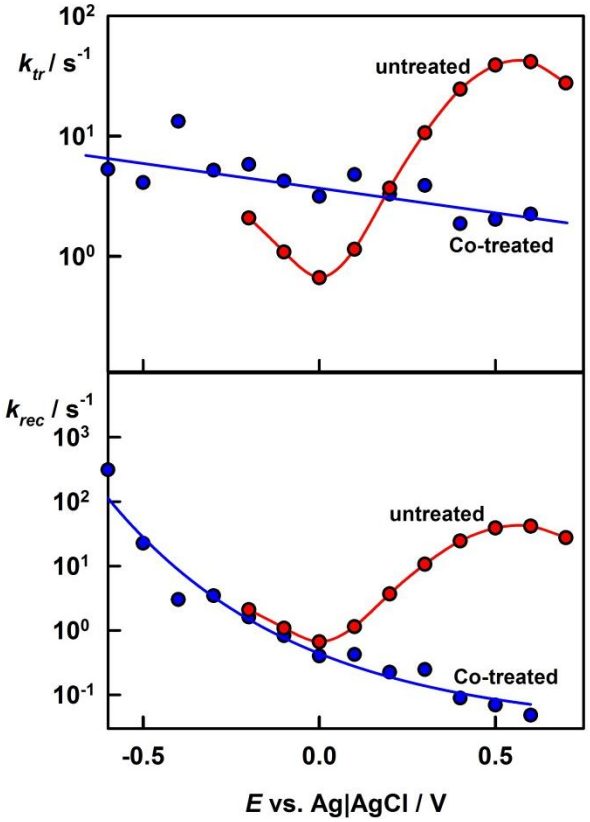

Figure 12. Rate constants for charge transfer and recombination for untreated and Co(II)-treated hematite film electrodes. Electrolyte 1.0 M NaOH. Illumination 455 nm, 11 mW cm^{-2}. The treatment involved placing a drop of 10mM cobalt nitrate solution on the electrode surface for 60s, followed by rinsing with pure water for 30s.

Photoelectrochemical Impedance Spectroscopy (PEIS)

The theory of photoelectrochemical impedance spectroscopy based on the simple kinetic scheme outlined above predicts that the impedance response of an illuminated semiconductor photoanode will exhibit two semicircles in the complex plane [30]. The theory assumes that the main influence of the potential modulation is to alter the recombination rate by changing the concentration of electrons at the surface. In the basic theory, it is assumed that the flux of holes, J_h, remains constant to a first approximation. It is also assumed that the potential modulation does not affect k_{tr}. In the case that $Csc << C_H$, the low frequency semicircle corresponds to a parallel RC network with the values

$$R_{LF} = \frac{k_B T}{q^2 J_h}\left(\frac{k_{tr} + k_{rec}}{k_{tr}}\right) \qquad (14a)$$

$$C_{LF} = \frac{q^2 J_h}{k_B T} \frac{1}{\left(k_{tr} + k_{rec}\right)} \tag{14b}$$

$$\omega_{\max,LF} = \frac{1}{R_{LF} C_{LF}} = k_{tr} \tag{14c}$$

The high frequency semicircle corresponds to a second parallel RC network with values

$$R_{HF} = \frac{k_B T}{q^2 J_h} \left(\frac{k_{tr} + k_{rec}}{k_{rec}} \right) \tag{15a}$$

$$C_{HF} = C_{sc} \tag{15b}$$

$$\omega_{\max,HF} = \frac{q^2 J_h}{k_B T C_{sc}} \left[\frac{k_{rec}}{k_{rec} + k_{tr}} \right] \tag{15c}$$

The theory originally presented in ref [30] has been re-derived and extended by Leng et al.[32] to include the effects of surface states and partial Fermi level pinning, which is expected to introduce a potential dependence in k_{tr} given by the Butler Volmer equation. The resulting expressions for the impedance are cumbersome, and the interested reader is referred to the original paper for details. Alternative approaches to the analysis of PEIS spectra have also been proposed that are based on equivalent circuits in which the resistors and capacitances correspond to distinct physical processes [13,14,33,34]. It is important to note that these approaches are not equivalent to the simple kinetic approach taken here.

Fig. 12 illustrates the main features of the PEIS response predicted by the theory.

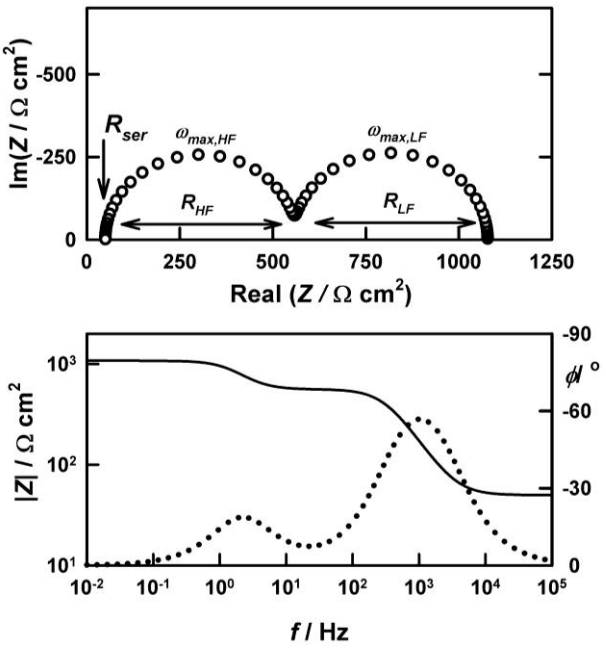

Figure 12. PEIS response predicted for $k_{tr} = k_{rec} = 10^2$ s^{-1}, $J_h = 10^{15}$ cm^{-2} s^{-1}, $C_{sc} = 1$ μF cm^{-2}, $C_H = 100$ μF cm^{-2}. The upper complex plane plot shows the two semicircles, and the lower Bode plot shows the separation of the low and high frequency *RC* time constants (continuous line: magnitude; broken line: phase).

Fig. 13 shows a typical experimental response for a hematite thin film photoanode. The two semicircles can be seen, but they are both flattened compared with the ideal response. In principle, the fitting can be improved by replacing the capacitances by constant phase shift elements, but this approach is inadvisable since it introduces additional arbitrary fitting parameters that have no physical meaning. The figure shows the reasonably satisfactory fit to two parallel *RC* elements connected in series with the ohmic resistance. In practice, it is the low frequency semicircle that is most important for extraction of k_{tr} and k_{rec} values.

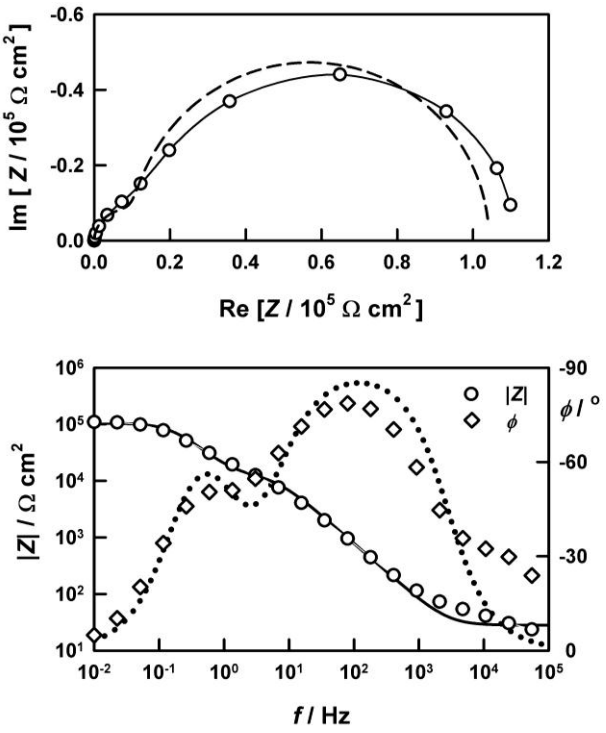

Figure 13. Typical experimental PEIS response for a thin film hematite photoanode. Electrolyte 1. NaOH. Potential 0.1 V vs. Ag|AgCl. Illumination 455 nm, ca.1 mW cm^{-2}.

Fig 14. Shows the calculated potential dependence of R_{LF} and C_{LF} in the photocurrent onset region for the ideal case where the potential dependence of the surface recombination rate constant k_{rec} is given by eqn. 8 and k_{tr} is independent of potential.

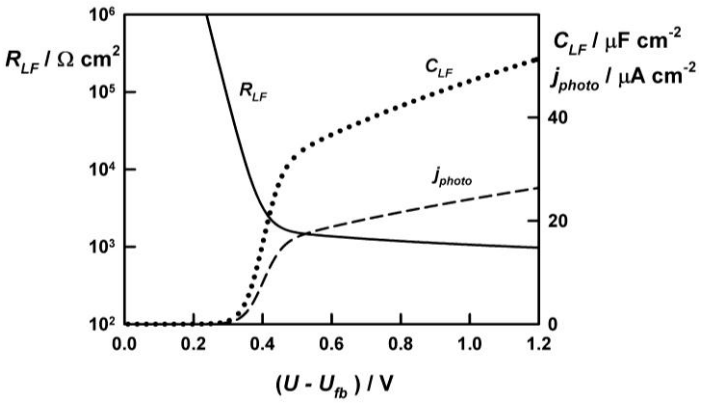

Figure 14. Potential dependence of R_{LF} and C_{LF} calculated from eqn. 14 using values of J_h and k_{rec} calculated using eqn. 9 and eqn. 8 respectively. Other values used in the calculation: $k_t = 20$ s^{-1}, $\alpha = 1.5 \times 10^5$ cm^{-1}, $N_d = 10^{19}$ cm^{-3}, $\varepsilon = 25$, $C_H = 100$ μF cm^{-2}, $\sigma_p = 10^{-16}$ cm^2, $\upsilon_{th} = 10^5$ cm s^{-1}, $I_0 = 2 \times 10^{15}$ cm^{-2} s^{-1}.

The experimental dependence of R_{LF} and C_{LF} on potential for untreated hematite electrodes is shown in Fig. 15, along with the derived values of the rate constants k_{tr} and k_{rec}. It can be seen that the potential dependence of k_{rec} has the same sinusoidal form seen in Fig 12, although in this case k_{tr} does not show such a pronounced maximum.

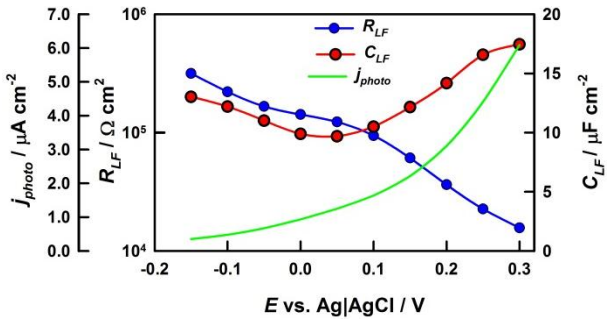

(a)

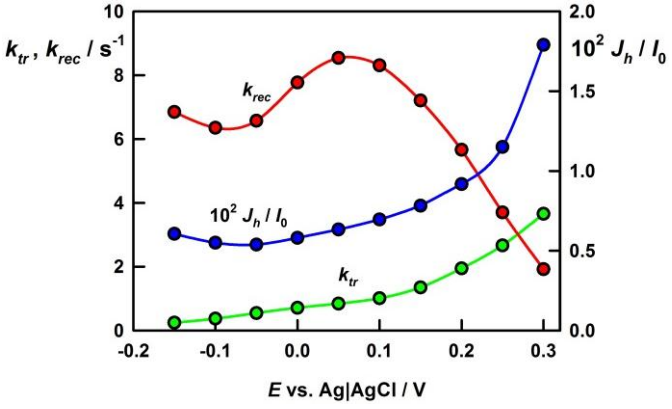

(b)

Figure 15. (a) Experimental values of R_{LF} and C_{LF} for an untreated hematite electrode. Electrolyte 1.0 M NaOH. Illumination 455 nm, ca. 1 mW cm^{-2}.

The approach given here is appropriate for bulk (i.e. compact) semiconductor films. It takes no account of electron or hole trapping in the bulk and it assumes that a space charge region is formed. An alternative approach,[35] which neglects space charge effects and introduces electron and hole trapping, may be more appropriate for mesoporous films in which the particles are completely depleted, but it is not applicable to continuous films of the type studied here.

Conclusions and Outlook

The preceding discussion highlights the fact that the consideration of kinetics and mechanisms for multiple electron transfer reactions at illuminated semiconductors is a subject that is still in its infancy. Progress towards the realization of efficient light-driven water splitting requires a better understanding of the chemical nature and energy landscape of the solid/electrolyte interface under illumination. A key issue is catalysis. Initially it was believed that the improvement of the photocurrent voltage behaviour produced by treatment of hematite electrodes with Co(II) was due to catalysis of hole transfer (i.e. an increase in k_{tr}). However, the results shown in Fig. 12 shows that k_{tr} is actually smaller for the cobalt-treated electrode. The improvement therefore arises from suppression of surface recombination. Further work is needed to identify catalysts that promote hole transfer to the electrolyte without increasing surface recombination. Identification of intermediates and the study of their temporal evolution under non steady-state conditions using advanced spectroscopic methods will also be an essential step towards relating the phenomenological rate constants discussed in the present paper with the elementary processes taking place during oxygen evolution. Much remains to be done before a viable system for water splitting based on materials like hematite can be developed.

Acknowledgments

The author thanks Dr Upul Wijayantha and members of his research group for their collaborative work on hematite electrodes.

References

1. Fujishima A, Honda K (1972) Nature 238: 37-38

2. Nozik AJ (1977) Bulletin of the American Physical Society 22: 95-95

3. Grätzel M, Augustyski J (2005) US Patent 6936143

4. Bolton JR, Strickler SJ, Connolly JS (1985) Nature 316: 495-500

5. Nakamura R, Nakato Y (2004) J. Am. Chem. Soc. 126: 1290-1298

6. Nakamura R, Okamura T, Ohashi N, Imanishi A, Nakato Y (2005) J Am Chem Soc 127: 12975-12983

7. Kay A, Cesar I, Graetzel M (2006) J. Am Chem Soc 128: 15714-15721

8. Barroso M, Cowan AJ, Pendlebury SR, Graetzel M, Klug DR, Durrant JR (2011) J Am Chem Soc 133: 14868-14871

9. Cowan AJ, Barnett CJ, Pendlebury SR, Barroso M, Sivula K, Graetzel M, Durrant JR, Klug DR (2011) J Am Chem Soc 133: 10134-10140

10. Dotan H, Sivula K, Graetzel M, Rothschild A, Warren SC (2011) Energy & Environ Sci 4: 958-964

11. Sivula K, Le Formal F, Graetzel M (2011) ChemSusChem 4: 432-449

12. Wijayantha KGU, Saremi-Yarahmadi S, Peter LM (2011) PCCP 13: 5264-5270

13. Klahr B, Gimenez S, Fabregat-Santiago F, Bisquert J, Hamann TW (2012) Energy & Environ Sci 5: 7626-7636

14. Klahr B, Gimenez S, Fabregat-Santiago F, Hamann T, Bisquert J (2012) J Am Chem Soc 134: 4294-4302

15. Peter LM, Ponomarev EA, Fermin DJ (1997) J Electroanal Chem 427: 79-96

16. Gärtner WW (1959) Phys Rev 116: 84

17. Wilson RH (1977) J Appl Phys 48: 4292-4297

18. Butler MA, Ginley DS (1980) J Mat Sci 15: 1-19

19. Reichman J (1980) Appl Phys Lett 36: 574-577

20. El Guibaly F, Colbow K (1983) J Appl Phys 54: 6488-6491

21. Li J, Peat R, Peter LM (1984) J Electroanal Chem 165: 41-59

22. Peter LM, Wijayantha KGU, Tahir AA (2012) Faraday Discuss 155:

23. Cass MJ, Duffy NW, Peter LM, Pennock SR, Ushiroda S, Walker AB (2003) J Phys Chem B 107: 5857-5863

24. Cummings CY, Marken F, Peter LM, Tahir AA, Wijayantha KGU (2012) Chem Commun 48: 2027-2029

25. Cummings CY, Marken F, Peter LM, Wijayantha KGU, Tahir AA (2012) J Am Chem Soc 134: 1228-1234

26. Peter LM, Vanmaekelbergh D(1999) Time and frequency resolved studies of photoelectrochemical kinetics. Adv Electrochem Sci Eng vol. 6 pp. 77-163. Weinheim

27. Peter LM, Li J, Peat R (1984) J Electroanal Chem 165: 29-40

28. Li J, Peter LM (1985) J.Electroanal Chem 193: 27-47

29. Peter LM, Li J, Peat R, Lewerenz HJ, Stumper J (1990) Electrochim Acta 35: 1657-1664

30. Ponomarev EA, Peter LM (1995) J Electroanal Chem. 397: 45-52

31. Peat R, Peter LM (1987) Ber Bunsen-Ges Phys Chem 91: 381-386

32. Leng WH, Zhang Z, Zhang JQ, Cao CN (2005) J Phys Chem B 109: 15008-15023

33. Schefold J (1992) J Electroanal Chem 341: 111-136

34. Schefold J (1995) J Electroanal Chem 394: 35-48

35. Bertoluzzi L, Bisquert (2012) J Phys. Chem Lett 3: 2517